Shift in the chemical composition of dissolved organic matter in the Congo River network

Thibault Lambert[1,*], Steven Bouillon[2], François Darchambeau[1], Philippe Massicotte[3], and Alberto V. Borges[1]

[1] University of Liège, Chemical Oceanography Unit, Liège, Belgium

[2] K.U. Leuven, Department of Earth and Environmental Sciences, Leuven, Belgium

[3] Aarhus University, Department of Bioscience, Denmark

* Corresponding author

Abstract. The processing of terrestrially derived dissolved organic matter (DOM) during downstream transport in fluvial networks is poorly understood. Here, we report a dataset of dissolved organic carbon (DOC) concentrations and DOM composition (stable carbon isotope ratios, absorption and fluorescence properties) acquired along a 1700 km transect in the middle reach of the Congo River Basin. Samples were collected in the mainstem and its tributaries during high water (HW) and falling water (FW) periods. DOC concentrations and DOM composition along the mainstem were found to differ between

the two periods, because of a reduced lateral mixing between the central water masses of the Congo River and DOM-rich waters from tributaries and also likely because of a greater photodegradation during FW as water residence time (WRT) increased. Although the Cuvette Centrale wetland (one of the world's largest flooded forest) continuously releases highly aromatic DOM in streams and rivers of the Congo Basin, the downstream transport of DOM was found to result in an along stream gradient from aromatic to aliphatic compounds. The characterization of DOM through parallel factor analysis (PARAFAC) suggests that this transition results from (1) the losses of aromatic compounds by photodegradation and (2) the production of aliphatic compounds by biological reworking of terrestrial DOM. Finally, this study highlights the critical importance of the river-floodplain connectivity in tropical rivers in controlling DOM biogeochemistry at large spatial scale and suggests that the degree of DOM processing during downstream transport is a function of landscape characteristics and WRT.

1. Introduction

Dissolved organic matter (DOM) is composed of thousands of heterogeneous compounds that differ in origin and reactivity (Leehneer and Croué, 2003) and is a central component of the global carbon cycle (Battin et al., 2008). DOM in streams and rivers mainly originates from the terrestrial ecosystem, but can also be fueled by internal sources (Bertilsson and Jones, 2003; Battin et al., 2008). Recent experimental and field studies have demonstrated that sorption, photochemical and biodegradation processes continuously degrade and transform DOM throughout fluvial networks (Massicotte and Frenette, 2011; Ward et al., 2013; Cory et al., 2014; Fasching et al., 2014; Lapierre and del Giorgio, 2014; Lambert et al., 2016). Large surveys of boreal lakes have suggested

45 that DOM was degraded along a gradient from aromatic to aliphatic compounds and that
46 the chemical composition of DOM was the dominant control of overall DOM reactivity
47 (Kothawala et al., 2014; Kellerman et al., 2015). Similarly, a large survey of temperate
48 streams and rivers has reported a preferential loss of aromatic DOM and parallel gain in
49 aliphatic DOM with increasing stream order, resulting in a diminution of the variability in
50 dissolved organic carbon (DOC) concentration and DOM composition from small
51 headwater streams to large rivers (Creed et al., 2015). However, the role of environmental
52 factors (i.e. climatic variables, water chemistry, landscape properties) on DOM
53 transformation in fluvial networks remains poorly constrained (Massicotte and Frenette,
54 2011; Marín-Spiotta et al., 2014).

55 The consideration of temporal dynamics in addition to the spatial dimension is
56 poorly investigated, yet it represents a crucial step towards a better understanding of DOM
57 transport and processing in fluvial networks. Temporal dynamics refer here to the changes
58 of the hydrological state of catchments that occur between high flow and low flow periods
59 and are susceptible to alter DOM dynamics for at least two reasons. First, the
60 concentration, the composition and the reactivity of DOM in streams and rivers are largely
61 determined by seasonal changes in water levels that control the hydrological connectivity
62 between rivers and wetlands (Junk et al., 1989; Battin, 1998; Besemer et al., 2009; Osburn
63 et al., 2009; Lambert et al., 2016). Secondly, the increase in water discharge during high
64 flow periods induces a decrease in water residence time (WRT) within catchments due to
65 increasing water velocities. Beyond the role of external and intrinsic drivers on DOM
66 degradation, WRT represents a major control that regulates the degree of DOM
67 transformation in aquatic ecosystems (Cory et al., 2007; Battin et al., 2008; Weyhenmeyer
68 et al., 2012). According to the recent pulse-shunt concept (Raymond et al., 2016) that

69 builds off on the “active pipe” concept (Cole et al., 2007), the degree of DOM processing
70 in fluvial networks should be reduced during high flow periods as hydrological events favor
71 the transport of DOM through the drainage network and therefore reduce the time where
72 dynamic processes can take place.

73 African tropical rivers have among the highest specific flux of DOC worldwide
74 (Meybeck, 1993) and have an important role in the global carbon cycle (Borges et al.,
75 2015a; 2015b). Yet, they remain largely underrepresented in large-scale studies on DOM
76 processing. For example, only few studies have investigated DOM biogeochemistry in the
77 Congo Basin (Spencer et al., 2010, 2012; Bouillon et al., 2012, 2014; Mann et al., 2014)
78 despite the fact that the Congo River – the largest river in Africa and the second largest
79 river worldwide after the Amazon in terms of drainage basin area and water discharge
80 (Laraque et al., 2009) – is the second major exporter of terrestrial organic carbon to the
81 oceans, 85-90% being in the form of DOC (Coynel et al., 2005; Laraque et al., 2009).
82 Downstream transport of DOM in the Congo River has not yet been investigated in its
83 middle reach where is located the second largest tropical flooded forest wetland, the
84 Congolese ‘Cuvette Centrale’. Additionally the Congo River receives in the middle reach
85 inputs from its major tributaries such as the Kasai, Ruki and Oubangui (Fig. 1).

86 Emerging conceptual models that describe how inland waters transform DOM
87 flowing down the fluvial network, such as the “chemostat” hypothesis (Creed et al., 2015)
88 and the pulse-shunt concept (Raymond et al., 2016), need to be tested by empirical data
89 acquired through extensive studies in tropical ecosystems. The Congo River and its
90 tributaries were sampled along a 1700 km transect from the city of Kisangani to the city of
91 Kinshasa during two contrasting hydrological periods (Figs. 1 and 2). DOM was
92 characterized through its optical properties, its stable carbon isotope composition

($\delta^{13}C_{DOC}$) and its DOC concentration. Optical measurements (including absorption and fluorescence) have been underscored as an efficient tool for characterizing the source and the reactivity of specific fractions of the DOM pool at large spatial scales (Jaffé et al., 2008; Yamashita et al., 2010; Massicotte and Frenette, 2011, Cawley et al., 2012; Kothawala et al., 2014; Lambert et al., 2016), notably with the development of multicomponent deconvolution techniques such as the parallel factor analysis (PARAFAC) (Stedmon et al., 2003; Murphy et al., 2013). The aims of this study were (1) to characterize the longitudinal evolution of DOM in the Congo River in the middle reach of the basin, (2) to investigate the transformation of DOM during its downstream transport in the fluvial network and (3) to identify potential environmental drivers of DOM processing.

2. Materials and Methods

2.1 Study area.

The Congo is the largest river in Africa and the second largest river in the world after the Amazon in terms of drainage basin area (~3.7 x 10^6 km²) and water discharge (~43 000 $m^3 s^{-1}$) (Laraque et al., 2009). The river originates in the southeastern part of the basin, and is called the Lualaba until it crosses the city of Kisangani and becomes known as the Congo. The Congo basin straddles the Equator, with major tributaries located in both hemispheres (Fig. 1). Thus, the rainy season on the northern part is compensated by the dry season on the southern part, and *vice-versa*. Consequently, seasonal water height variations are largely attenuated (Runge, 2008), in stark contrast with the Amazon river, leading to marked differences in biogeochemistry (e.g. CH_4 dynamics, Borges et al., 2015b) and aquatic ecology (e.g. phytoplankton development, Descy et al., 2016) between these two rivers. The hydrological cycle of the Congo River at Kisangani and

Kinshasa is similar, with a bimodal distribution: maximum water peaks occur in December and May and minimum flow in August and March (Fig. 2). The center of the basin is covered by evergreen forest (~50% of the total area), and surrounded by savannah on the northern and southern rims of the catchment. The Cuvette Centrale is located in the central part of the basin on both side of the Equator and consists mainly in a vast permanently flooded forested area of 360 x 10^3 km² (Bwangoy et al., 2010). The core of the Cuvette Centrale corresponds to the net increase in the wetland fraction along the Congo River as the mainstem connects with large tributaries flowing through the flooded forest (Fig. 1 and Supplementary Fig. 1). The most important tributaries of the Congo in terms of discharge are the Oubangui (4200 $m^3 s^{-1}$) and the Sangha (2220 $m^3 s^{-1}$) on the northern side, the Kasai (9000 $m^3 s^{-1}$) on the southern side, and the Ruki (3950 $m^3 s^{-1}$) and the Lulonga (2040 $m^3 s^{-1}$) along the Equator (Bricquet, 1995; Coynel et al., 2005; Laraque et al., 2009).

2.2. Field data collection.

Samples were collected during the yearly discharge maximum in December (03-19 December 2013; high waters (HW)) and during falling waters (FW) following the second discharge maximum occurring in March (10-30 June 2014) (Fig. 2). As water level of the Congo River follows similar seasonal fluctuations at Kisangani and Kinshasa (Fig. 2), the timing of high and low waters was likely similar for the sites located along the mainstem. WRT between Kisangani and Kinshasa has been roughly estimated to increase by about ~5 days during FW compared to HW (Descy et al., 2016) but is likely not uniform along the transect: because the main tributaries are all located downstream, the increase of WRT is probably more important upstream of the Oubangui. Water samples were collected in the Congo River itself as well as in small and large tributaries at the confluence

(Table 1). Stations along the mainstem were located ~50 km apart from Kisangani to Kinshasa. Major tributaries included the Tshopo, the Lindi, the Itimbiri, the Aruwini, the Mongala, the Oubangui, the Sangha and the Lefini on the right bank of the Congo, and the Lomami, the Lulonga, the Ikelemba, the Ruki and the Kwa/Kasai on the left bank. The Lefini was sampled only during the first campaign (high waters).

Water sampling was performed from a 22 m boat on the mainstem and with a canoe in the tributaries. Approximately 2 L of water were collected 0.5 m below the surface, stored away from direct sunshine and filtered and conditioned typically within 15 min of sampling. Filtrations were performed successively on pre-combusted GF/F glass fiber filters (0.7 µm porosity), then on 0.2 µm polyethersulfone syringe filters. Samples for the measurement of DOC concentrations and $\delta^{13}C_{DOC}$ signatures were stored in 40 mL glass vials with polytetrafluoroethylene (PTFE) coated septa with 50 µL H_3PO_4 (85%). Samples for colored DOM (CDOM) and fluorescent DOM (FDOM) analyses were stored in 20 mL amber glass vials with PTFE-coated septa but without H_3PO_4 addition. Samples for CDOM and FDOM were stored just after filtration at 4°C in a refrigerator on the boat until transportation back to Belgium, where they were also stored at 4°C until analysis within one week of arrival. Potential storage and degradation effects were assessed by analyzing a series of contrasting samples after 3 months (Supplementary Fig. 2). The differences in optical proxies (a_{350}, $SUVA_{254}$ ad S_R) were less than 5% (n=22) and no significant changes were observed by comparing excitation-emission matrices (EEMs). Samples for major elements (including Fe) were stored in 20 mL scintillation vials and acidified with 50 µl of HNO_3 65 % prior to analysis.

Fe was measured by inductively coupled plasma spectrometry (Agilent 7700x ICP-MS). DOC and $\delta^{13}C_{DOC}$ were analyzed with an Aurora1030 total organic carbon analyzer

(OI Analytical) coupled to a Delta V Advantage isotope ratio mass spectrometer. Typical precision observed in duplicate samples was in >95% cases < ± 5 % for DOC, and ± 0.2 ‰ for $\delta^{13}C_{DOC}$. Quantification and calibration were performed with series of standards prepared in different concentrations, using both IAEA-C6 ($\delta^{13}C$ = -10.4 ‰) and in-house sucrose standards ($\delta^{13}C$=-26.9 ‰). All data are reported in the δ notation relative to VPDB (Vienna Pee Dee Belemnite). Absorbance was recorded on a Perkin-Elmer UV/Vis 650S spectrophotometer using a 1 cm quartz cuvette. Absorbance spectra were measured between 200 and 700 nm at 1 nm increment and instrument noise was assessed measuring ultrapure (Type 1) Milli-Q (Millipore) water as blank. After subtracting the blank spectrum, the correction for scattering and index of refraction was performed by fitting the absorbance spectra to the data over the 200-700 nm range according to the following equation:

$$A_\lambda = A_0 e^{-S(\lambda-\lambda_0)} + K \quad (1)$$

where A_λ and A_0 are the absorbance measured at defined wavelength λ and at reference wavelength λ_0 = 375 nm, respectively, S the spectral slope (nm^{-1}) that describes the approximate exponential decline in absorption with increasing wavelength and K a background offset. The fit was not used for any purpose other than to provide an offset value K that was then subtracted from the whole spectrum (Lambert et al., 2015). Fluorescence intensity was recorded on a Perkin-Elmer LS45 fluorescence spectrometer using a 1 cm quartz cuvette across excitation wavelengths of 220-450 nm (5 nm increments) and emission wavelengths of 230-600 nm (0.5 nm increments) in order to build EEMs. If necessary, samples were diluted until A_{254} < 0.2 m^{-1} to avoid problematic inner filter effects (Ohno, 2002). Before each measurement session (i.e. each day), a Milli-Q water sample was also measured and subtracted from EEMs.

188 Water temperature, $\%O_2$, and pH were measured *in situ* with portable field probes
189 calibrated using standard protocols (YSI ProPlus probe). Pelagic respiration (R) was
190 determined from the decrease of O_2 in 60 ml biological oxygen demand bottles over ~24
191 h incubation periods. The bottles were kept in the dark and close to *in situ* temperature in
192 a cool box filled with in situ water. The O_2 decrease was determined from triplicate
193 measurements at the start and the end of the incubation with an optical O_2 probe (YSI
194 ProODO). The respiratory quotient (RQ), defined as the molar ratio of O_2 consumed to
195 CO_2 produced by respiration, allows the conversion of respiration measurements from O_2
196 to C units. The RQ value is in theory equal to 1 for the oxidation of glucose, but higher
197 than 1 for more complex and reduced organic molecules, such as lipids and proteins (e.g.
198 1.3 in a temperate stream with a catchment dominated by pastures, Richardson et al.,
199 2013), or lower than 1 for highly oxidized and oxygen-rich molecules (e.g. 0.8 in boreal
200 lakes, Berggren et al. 2012). Given the range of RQ values, we adopted a RQ value of
201 1.0. The vertical light attenuation coefficient, K_d (m^{-1}), was calculated from simultaneous
202 measurements of surface irradiance with a Li-Cor LI-190 quantum sensor and underwater
203 photosynthetically active radiation (PAR) measurements with a submersible Li-Cor LI-
204 193SA spherical quantum sensor. K_d was derived from the slope of the semi-logarithmic
205 regression between relative quantum irradiance and depth. Transparency of the water
206 column was measured using a 20-cm diameter Secchi disk.

207 **2.3. Characterization of DOM composition.**

208 The specific ultra-violet absorbance ($SUVA_{254}$) was calculated as the UV
209 absorbance at λ = 254 nm (A_{254}) normalized to the corresponding DOC concentration
210 (Weishaar et al., 2003). The natural UV absorbance of Fe at λ = 254 nm was estimated
211 based on measured Fe concentrations and was then subtracted from the UV absorbance

measured. The corrected value of A_{254} was then used to calculate $SUVA_{254}$. The $SUVA_{254}$ was used as an indicator of the aromaticity with higher values indicative of greater percent of aromaticity (Weishaar et al., 2003).

Napierian absorption coefficients were calculated according to:

$$a_\lambda = 2.303 \times A_\lambda / L \quad (2)$$

where a_λ is the absorption coefficient (m^{-1}) at wavelength λ, A_λ the absorbance corrected at wavelength λ and L the path length of the optical cell in m (0.01 m). CDOM was reported as the absorption coefficient at 350 nm (a_{350}). Spectral slopes for the intervals 275-295 ($S_{275-295}$) nm and 350-400 nm ($S_{350-400}$) were determined from the linear regression of the log-transformed *a* spectra versus wavelength. The slope ratio S_R was then calculated as the ratio of $S_{275-295}$ to $S_{350-400}$. S_R is inversely related to the molecular weight (MW) distribution of DOM (Helms et al. 2008). The fluorescence index (FI) was calculated as the ratio of the emission intensities at 470 nm and 520 nm at an excitation wavelength of 370 nm (McKnight et al., 2001). A higher FI value (e.g., 1.8) indicates an aquatic microbial DOM source while a lower value (e.g., 1.2) indicates a terrestrial source. Intermediate values indicate a mixed DOM source.

2.4. PARAFAC modeling.

EEMs preprocessing (including removing first and second Raman scattering, standardization to Raman units, absorbance corrections and inner filter effects) was performed prior the PARAFAC modeling. The scans were standardized to Raman units (normalized to the integral of the Raman signal between 390 nm and 410 nm in emission at a fixed excitation of 350 nm) with a Milli-Q water sample run the same day as the samples (Zepp et al., 2004). PARAFAC model was build using MATLAB (MathWorks, Natick, MA, USA) and the drEEM Toolbox version 1.0 (Murphy et al., 2013). Validation of

the model was performed by split-half analysis and random initialization. The normalization step was applied to scale each EEM to its total signal, thus ensuring the model focused entirely on compositional rather than concentration gradients. Additional samples analyzed in the same manner and collected from the Kwa/Kasai river basin (n = 104), Lago Janauacá (a central Amazon floodplain lake, n = 17), the Niger River (n = 19) and the Okavango delta (n = 17) were added to the dataset to increase the variability of DOM fluorescence signatures and help detect components that could have been present in insufficient quantity to be detected in our environment. The maximum fluorescence F_{Max} values of each component for a particular sample provided by the model were summed to calculate the total fluorescence signal F_{Tot} of the sample in Raman unit (R.U.). The relative abundance of any particular PARAFAC component X was then calculated as $\%C_X = F_{Max}(X) / F_{Tot}$.

The positions of maximum peaks established by the model were compared to the classical excitation-emission matrices nomenclature (Fellman et al., 2010; Coble et al., 2014) and with other reported PARAFAC models built in a large variety of freshwater ecosystems (Table 2). Additionally, each PARAFAC component was associated to a dominant molecular class based on recent studies aiming to correlate individual molecular formula with different PARAFAC components through Fourier transform ion cyclotron resonance mass spectrometry (FTICR-MS). Such studies have been carried out in Swedish lakes (Kellerman et al., 2015), boreal streams and rivers (Stubbins et al., 2014) and a subtropical wetland (Wagner et al., 2015). Although such comparison has not been performed with our own samples, the relatively good consistency of associations between optical and molecular linkages observed in these contrasting environments suggests that PARAFAC components can track dominant DOM molecular composition similarly across

different biomes in terms of DOM MW and enrichment in aliphatic or aromatic molecules (Wagner et al., 2015).

2.5. Landscape analysis.

The total drainage area and the Strahler stream order (Strahler, 1957) were calculated at each station in the geographic information system (GIS) software ArcGis® (ESRI 2011, ArcGis Desktop 10.3.1), using the ArcHydro tools (v. 2.0) and the hydrological data and maps based on shuttle elevation derivatives at a 3" resolution (Lehner et al., 2008). The extent of wetland areas and flooded dense forest cover were extracted from the Global Lakes and Wetlands Database (Lehner and Döll, 2004) and from Global Land Cover 2009 database (Bontemps et al. 2011), respectively.

2.6 Statistical Analysis.

Mann-Whitney t-tests were performed to investigate differences in DOM properties spatially (mainstem *versus* tributaries) and temporally (HW *versus* FW). A principal component analysis (PCA) was also performed to explore DOM evolution during its transport through the Congo fluvial network. The optical properties of DOM including level of CDOM (a_{350}), bulk composition ($SUVA_{254}$, S_R, FI) and the relative abundance of PARAFAC components were used as the variables. Given the different units of these variables, data were scaled to zero-mean and unit-variance as recommended (Borcard et al., 2011). The PCA was performed using the prcomp function in R software.

3. Results

3.1. DOC concentrations and DOM bulk composition.

DOC concentrations in the mainstem were higher during HW (5.4 – 13.9 mg L^{-1}, average 8.2±2.6 mg L^{-1}) compared to FW (4.2 – 9.8 mg L^{-1}, average 5.9±1.8 mg L^{-1}) but showed similar longitudinal patterns during both hydrological periods (Fig. 3a, 3b): DOC

284 increased slowly in the upper part of the transect (0.0012 mgDOC km^{-1} at HW and 0.0002
285 mgDOC km^{-1} at FW) and then faster as the Congo River evolved throughout the core of
286 the Cuvette Centrale and mixed with the Kwa/Kasai River (0.0091 mgDOC km^{-1} at HW
287 and 0.0085 mgDOC km^{-1} at FW) (Fig. 1). The breaking point in the DOC longitudinal
288 increase in DOC concentrations was located around km 700 during HW, and km 500
289 during FW. DOC concentrations in tributaries were highly variable (from 1.8 to 67.8 mg L^{-1})
290 and were found to be correlated with the extent of flooded forest (Fig. 4), resulting in
291 highest concentrations in tributaries draining the Cuvette Centrale and lowest
292 concentrations in those draining savannah areas upstream of Kinshasa (Fig. 1).
293 Tributaries located downstream of the Cuvette Centrale were also characterized by lowest
294 DOC concentrations during FW compared to HW while no clear pattern was observed for
295 those located upstream.

296 $\delta^{13}C_{DOC}$ signatures in the mainstem were lower during HW (from -30.6 to -28.8 ‰,
297 average -29.4±0.3 ‰, *n* = 35) compared to FW (from -29.3 to -25.2 ‰, average -27.5±0.9
298 ‰, *n* = 34). $\delta^{13}C_{DOC}$ during HW decreased about 0.7 ‰ from Kisangani to km ~ 1200,
299 remained stable until km ~ 600 and then increased slightly towards Kinshasa. During FW,
300 $\delta^{13}C_{DOC}$ decreased markedly about 3 ‰ between Kisangani and km ~ 1600. Downstream,
301 values were variable (-27.2±0.6 ‰ between km 600 – 1600, *n* = 18) and then showed ~ 1
302 ‰ drops at km ~ 600 and ~ 200, coinciding with the confluence zones with the Oubangui
303 and the Kwa/Kasai rivers, respectively. In tributaries, $\delta^{13}C_{DOC}$ values displayed a similar
304 pattern during the two hydrological periods with low and relatively stable values (-29.7±0.5
305 ‰, *n* = 76) in streams and rivers draining dense forest areas and higher signatures in
306 those flowing savannah areas 0-400 km upstream of Kinshasa (-28.1±0.8, n = 14).
307 Stations of the mainstem located within or upstream the Cuvette Centrale were

characterized by highest $\delta^{13}C_{DOC}$ values than those measured in tributaries collected along the same transect, both during HW ($p < 0.004$) and FW ($p < 0.0001$). Downstream the Cuvette Centrale, stations of the mainstem had lower $\delta^{13}C_{DOC}$ signatures than those measured in tributaries ($p < 0.0001$, all periods).

$SUVA_{254}$ and S_R during both periods varied mainly between 4.0 – 5.2 L mgC^{-1} m^{-1} and 0.734 – 0.802 among all stations, respectively (10% – 90% percentiles, n=160), indicating that DOM in the Congo basin was dominated by aromatic compounds of high MW during both periods (Fig. 3e-3h). $SUVA_{254}$ generally decreased from Kisangani to Kinshasa in the mainstem during HW, with a slight increase between km 500 and 800 upstream of Kinshasa, while S_R exhibited stable values from Kisangani and then started to increase towards Kinshasa at km 700. Compared to HW, $SUVA_{254}$ during FW was relatively stable and lowest from Kisangani to km 500 but higher between km 0 – 500 as $SUVA_{254}$ increased markedly in this section ($p < 0.0001$). S_R exhibited a hump-shaped pattern during FW, with increasing values from Kisangani to km 500 and decreasing value between km 0 – 500. A slight decrease in $SUVA_{254}$ ($p = 0.0043$) associated with an increase in S_R ($p = 0.047$) was also observed between km 200 – 400. Generally, $SUVA_{254}$ in tributaries were slightly higher at FW than at HW ($p = 0.035$), similar to the mainstem in HW but higher in FW ($p = 0.0113$). FI in the mainstem gradually decreased from Kisangani to Kinshasa during both hydrological periods, with higher values during FW than at HW ($p = 0.0006$), and were highest than in tributaries ($p < 0.0001$). No distinct seasonal variation was apparent in tributaries.

3.2. PARAFAC results.

Six PARAFAC components were determined to adequately model our dataset (Table 2, Supplementary Fig. 3). Components C1, C3, C4, and C5 are all classified as

"humic-like" but differ in terms of sources, molecular association and reactivity (Table 2). C1 and C3 are commonly reported in freshwaters and are associated with a group of high MW and aromatic molecules of terrestrial origin (e.g. Wagner et al., 2015). Both are susceptible to photodegradation (Lapierre and del Giorgio, 2014). C4 is associated with terrigenous molecules of lower aromaticity and MW relative to C1 and C3 (Kellerman et al., 2015). C4 commonly originates from terrestrial inputs (Stedmon and Markager, 2005; Yamashita et al., 2010; Lambert et al., 2016), and has been shown to be resistant to photodegradation (Massicotte and Frenette, 2010; Ishii and Boyer, 2012). Among the humic-like compounds, C5 is associated with molecules characterized by lowest aromaticity and MW produced during the photodegradation of terrestrial DOM (Lapierre and del Giorgio, 2014; Stubbins et al., 2014). C2 and C6 are classified as microbial humic-like and tryptophan-like components, respectively (Fellman et al., 2010). In contrast to the other components, C2 and C6 are associated with low MW DOM fractions enriched in aliphatic molecules biologically produced within aquatic ecosystems (Kellerman et al., 2015; Wagner et al., 2015). Both C2 and C6 can be assigned to a fraction of DOM produced during the microbial degradation of terrestrial DOM within freshwaters (Stedmon et al., 2003; Walker et al., 2013), although autochthonous primary production represents another potential source for C6 (Yamashita et al., 2010).

The relative contribution of C1 and C3 showed similar patterns along the mainstem during both periods (Fig. 5). %C1 and %C3 during HW presented a slight downstream decrease followed by an increase with minimal contribution recorded around km 1100. %C1 and %C3 were lowest during FW ($p = 0.017$ and $p < 0.0001$, respectively), with low variability upstream of km 500 and highest contribution downstream. %C4 displayed a general increase along the transect at HW especially marked between Kisangani and km

~1100 and between km 600 to km 150. During FW, the longitudinal evolution of %C4 showed an opposite pattern to those of %C1 and %C3, with a higher contribution than during HW ($p > 0.0001$). Overall, %C5 was higher during FW than during HW ($p < 0.0001$) and exhibited longitudinal patterns opposite to those of %C3 during both periods. %C2 was relatively stable along the mainstem during both periods, with higher contribution during FW compared to HW ($p = 0.0076$). C6 exhibited the lowest contribution to FDOM signal and %C6 trended to be lower during FW compared to HW. Longitudinal evolution of C6 was characterized by a strong drop along the mainstem, occurring around km 800 at HW and km 500 at FW.

Overall, tributaries were characterized by higher %C3 but lower %C2 and %C6 relative to the mainstem ($p < 0.0001$). %C4 and %C1 were higher ($p = 0.0007$) and lower ($p = 0.017$), respectively, in tributaries than in the mainstem during HW, and no difference was observed at FW. No difference was observed for %C5 between tributaries and the mainstem for both periods. The seasonal variability within tributaries was characterized by higher contribution of C4 ($p = 0.025$) and C5 ($p < 0.0001$) and lower contribution of C3 ($p = 0.0015$) and C6 ($p = 0.003$) during FW compared to HW.

3.3. PCA results.

The first two principal components (PC) accounted for 57% of the total variance (Fig. 6). The first PC (PC1) showed a transition from terrestrial aromatic DOM (%C3, $SUVA_{254}$, DOC, a_{350}, positive loadings) to aliphatic DOM (%C2, %C6, FI, negative loadings). Along the second PC (PC2), PARAFAC components are distributed with C1 and C3 as negative loadings and C4 and C5 as positive loadings. C1 and C3 have been identified as photo-sensitive (Yamashita et al., 2010; Lapierre and del Giorgio, 2014) while

C4 and C5 are considered as photo-resistant (Massicotte and Frenette, 2010; Ishii and Boyer, 2012) and produced by photodegradation (Lapierre and del Giorgio, 2014), respectively. Therefore, the PC2 can be interpreted as indicative of photodegradation (Cawley et al., 2012). The distribution of sampling stations for a given Strahler order was highly heterogeneous (Fig. 6a). However, a global pattern emerges along PC1 with stations collected in the mainstem showing mainly negative scores (Fig. 6b). Furthermore, stations of the mainstem collected during HW had negative scores along PC2, but positive scores during FW. Overall, stations collected during HW had mainly negative scores along PC2 while those sampled at FW showed large variability along PC2.

4. Discussion

4.1. Longitudinal evolution of DOM. From Kisangani to Kinshasa the Congo River continually receives DOM inputs from tributaries flowing through the Cuvette Centrale (Fig. 4), resulting in a net longitudinal increase in DOC concentrations during both periods. However the longitudinal evolution in DOM content and composition differed between the two campaigns due to the combination of several factors.

4.1.1. Seasonal changes in DOM sources mobilized in the upper basin. The large variation in $\delta^{13}C_{DOC}$ values in the mainstem at Kisangani between HW (-29.0 ‰) and FW (-25.2 ‰) can be related to a shift in the source of DOM mobilized in the upper part of the basin due to differences in water routing during the hydrograph. Thus, decreasing $\delta^{13}C_{DOC}$ signatures that occurred during high flow periods have been attributed to the mobilization of fresh DOM from superficial soil horizons in wide variety of catchments (Neff et al., 2006; Sanderman et al., 2009; Lambert et al., 2011; Bouillon et al., 2012). Higher $\delta^{13}C_{DOC}$ values during low flow periods reflect the deepening of water flow paths and the subsequent

mobilization of more degraded DOM from deeper soil horizons. This seasonal change in DOM composition at the start of the Kisangani – Kinshasa transect is further supported by an ongoing high frequency sampling carried out at Kisangani (own unpublished data).

4.1.2. Reduced lateral exchanges between the Congo River and the flooded forest during falling waters. The decreasing but higher $\delta^{13}C_{DOC}$ signatures in the mainstem compared to tributaries during FW indicate a reduced lateral mixing between the central water masses of the Congo River and DOM-rich waters from tributaries. Although we cannot rule out that lateral exchanges are likely driven by water level fluctuations in the Congo River, our data suggest that photodegradation of terrestrial DOM contributes to limit the downstream DOC enrichment during FW. Photodegradation is known to preferentially act on the colored, photosensitive molecules associated with high MW and aromaticity (Helms et al., 2008; Spencer et al., 2009; Lapierre and del Giorgio, 2014), and is expected to be highly efficient in aquatic ecosystems rich in light-absorbing CDOM such as the Congo River (Cawley et al., 2012; Cory et al., 2014). A stronger effect of DOM photodegradation in the mainstem during FW is supported by three lines of evidence in our data. First, C1 and C3 – both associated with highly aromatic molecules of high MW (Table 2) – were lower during FW compared to HW, and this decrease occurred along with a decrease in DOM aromaticity (lower $SUVA_{254}$) and increase in average MW (higher S_R) (Fig. 3 and 5). Second, the more drastic decrease in %C3 is consistent with the well documented high photosensibility of this component relative to other terrestrial humic-like components (Yamashita et al., 2010; Cawley et al., 2012; Lapierre and del Giorgio, 2014). Finally, the PCA analysis clearly separates stations collected in the mainstem between HW (negative scores) and FW (positive scores) along the PC2 which highlights that photodegradation is an important driver of DOM composition in the Congo Basin.

A stronger degree of DOM photodegradation during FW implies a higher exposure of CDOM to solar irradiation, either spatially (i.e. in the water column) or temporally. The higher coefficient of light attenuation in the water column (K_d) and lower Secchi depths during FW (Table 1) indicate that the penetration of sunlight in the water column was reduced compared to HW. This was likely due to the greater total suspended matter (TSM) concentrations (Table 1) and phytoplanktonic development (Descy et al. 2016), although CDOM likely remained the main driver of light penetration. Thus, the degree of DOM photodegradation appears to be mainly driven by changes in WRT that has been estimated to increase about ~5 days in FW compared to HW (Descy et al., 2016). Although sunlight depth penetration was low and the variation in the WRT relatively small, rates of photodegradation can be elevated in CDOM-rich ecosystems (Cory et al., 2015) and this process can substantially alter terrestrial DOM over short time scale (e.g. ~12h of sunlight alteration according to Cory et al., 2015). Further research is needed in order to quantify photodegradation rate and the relative importance of this process on C cycling in the Congo Basin, but this was beyond the scope of the present study.

4.1.3. Role of large tributaries and channel width in controlling the longitudinal evolution of DOM from Kisangani to Kinshasa. DOM enrichment was more pronounced within the core of the Cuvette Centrale (Fig. 2) that corresponds to the region where the major tributaries in terms of discharge (i.e. the Lulonga, the Ruki, the Sangha, the Oubangui and the Kwa/Kasai rivers) connect the mainstem. These tributaries are also very rich in terrestrial DOM from the large flooded forest (Coynel et al., 2005; Laraque et al., 2009) (Fig. 1 and Supplementary Fig. 1). DOC concentrations increased faster immediately as the Congo enters in this central part of the Cuvette Centrale during HW, reflecting the strong lateral mixing between water masses. However, the net rise in DOC

concentrations during FW was found to occur first at ~70 km downstream of the confluence zone with the Oubangui River, coinciding with a strong reduction of the channel width (Supplementary Fig. 4). The ~1 ‰ drop in $\delta^{13}C_{DOC}$ associated with changes in DOM composition (especially increase in $SUVA_{254}$ and %C3) at this station indicates that the reduction of the channel width favors the lateral mixing between the mainstem and waters from the Cuvette Centrale that travel along the river ridge lined by dense forest without being significantly impacted by photodegradation (Supplementary Fig. 5). In fact, a "complete" lateral mixing with waters from the Cuvette Centrale occurs after the confluence zone with the Kwa/Kasai River (based on cross channel transects of conductivity and pH, not shown). In this part of the river, the high discharge of the Kwa/Kasai combined with a narrow mainstem channel devoid of sand bars and islands (Runge et al., 2008) forces lateral mixing. This is supported by the fact that $\delta^{13}C_{DOC}$ signatures of the Congo mainstem became typical of black waters only after connecting with the Kwa/Kasai during FW, and could also explain why the DOC increase is greater at this point while DOC is typically higher in tributaries located more upstream (e.g. The Ruki River).

Large tributaries also controlled the general evolution of DOM composition from Kisangani to Kinshasa. DOM aromaticity ($SUVA_{254}$) decreased slightly along the transect during HW (from ~4.6 to 4.2 mgC L^{-1} m^{-1} from Kisangani to Kinshasa), but increased significantly during FW (from ~4.0 to 5.3 mgC L^{-1} m^{-1} from Kisangani to Kinshasa) due to an increase in DOM aromaticity in large tributaries flowing through or connected to the Cuvette Centrale.

4.2. DOM transformation during its downstream transport. Strahler stream order was used as an organizing concept for the individual characterization of stream reaches within

474 the network (Strahler, 1957, Poole, 2010), and in order to investigate DOM composition
475 across a gradient of streams and rivers. Although DOM in the Congo Basin is fairly
476 dominated by terrestrial inputs of aromatic DOM, the loadings plot along PC1 indicates a
477 transition in the dominant DOM composition from aromatic (%C3, $SUVA_{254}$) to aliphatic
478 (%C2, %C6, FI) compounds (Fig. 6). It is noteworthy that similar gradients have recently
479 been reported in Swedish lakes (Kellerman et al., 2015) and U.S. rivers networks (Creed
480 et al., 2015), suggesting that the large-scale governing processes controlling DOM in
481 freshwater are similar across biomes. However, the underlying mechanisms remain to be
482 elucidated. Thus, the gain in aliphatic DOM has been attributed to the increasing influence
483 of autochthonous sources (Creed et al., 2015) or to the degradation of terrestrial DOM
484 (Kellerman et al., 2015), while external factors (i.e. not related to DOM composition) have
485 been suggested to have little influence on this pattern (Kellerman et al., 2015). Our study
486 supports the hypothesis that the degradation of terrestrial DOM is the main driver on DOM
487 transformation in aquatic systems, but also highlights the role of landscape morphology
488 and environmental conditions in influencing the transition from an aromatic to aliphatic
489 dominant composition.
490 **4.2.1. Losses of aromatic DOM through photodegradation and biological activity as**
491 **producer of aliphatic DOM.** The role of photodegradation in removing the aromatic
492 fraction of DOM in the Congo Basin, strongly suggested by the PCA analysis as well as
493 by the changes in DOM composition along the mainstem between HW and FW, is also
494 supported by patterns in C5. Indeed, %C5 was inversely related to %C3 (Fig. 7a),
495 suggesting that C5 tracks molecules directly produced during the photodegradation of
496 terrestrial aromatic molecules as previously demonstrated in boreal freshwaters (Lapierre
497 and del Giorgio, 2014). In addition, %C5 was inversely related with measurements of

498 pelagic community respiration (R) performed concurrently with DOM sampling (Borges et
499 al., 2015a) and attributed to bacterial respiration since phytoplankton biomass is generally
500 low (Descy et al. 2016) (Fig. 7b). Given that C5 is associated with molecules of low MW
501 and aromaticity (Stubbins et al., 2014), this observation is consistent with experimental
502 results showing that the aromatic and high MW fraction of terrestrial DOM can be
503 photochemically converted into more labile substances of lower MW that in turn can
504 support the aquatic bacterial metabolism (Bano et al., 1998; Tranvik and Bertilsson, 2001;
505 Remington et al., 2011; Cory et al., 2014). The lack of correlation between %C5 and R in
506 the mainstem likely indicates an additional source of labile DOM. The higher
507 concentrations of chlorophyll-a in the mainstem compared to tributaries (Table 1) suggest
508 that this source could be phytoplanktonic exudates that have been shown to be very labile
509 and rapidly assimilated by bacteria (Baines and Pace, 1991; Morana et al., 2014).

510 The dual role of microorganisms as consumers of terrigenous aromatic DOM and
511 producers of novel compounds has recently been emphasized (Guillemette and del
512 Giorgio, 2012; Ward et al., 2013; Fasching et al., 2014) and could explain the gain in
513 aliphatic DOM in the Congo River. Components C2 and C6 – associated with aliphatic
514 molecules (Table 2) – exhibited systematically higher contributions in the mainstem
515 compared to tributaries, implying a permanent internal production. However, none of
516 these components were correlated to chlorophyll-a concentrations (data not shown),
517 suggesting that the phytoplankton primary production in the Congo basin was not
518 controlling their distribution. On the other hand, several studies carried out in a wide
519 variety of aquatic ecosystems have attributed the origin of components like C2 and C6 to
520 the biological degradation of terrestrial DOM within the aquatic ecosystems (Stedmon et
521 al., 2003; Yamshita et al., 2010; Walker et al., 2013; Fasching et al., 2014; Kellerman et

al., 2015). Therefore, microbial reworking of terrestrial DOM during its transport could lead to the production of these components, an assumption supported by higher FI values in the mainstem inferring greater inputs of microbially derived DOM relative to tributaries (McKnight et al., 2001).

Our results contrast with previous investigations based on lignin biomarkers suggesting that DOM transformation in the Congo basin is mainly driven by dynamic exchanges with the particulate organic carbon (POC) pool via sorption or leaching processes (Spencer et al., 2012; Mann et al., 2014). The $\delta^{13}C$ signatures of POC collected during our field campaigns spanned a much wider range but were poorly correlated with $\delta^{13}C_{DOC}$ ($R^2 = 0.20$, $p < 0.0001$; $n = 158$, data not shown), suggesting limited exchange between these pools. However, our results are in line with previous field studies showing that downstream changes in DOM composition can be largely controlled by photodegradation (Massicotte and Frenette, 2011; Cawley et al., 2012).

4.2.2. Role of external drivers on the aromatic towards aliphatic transition. The distribution of data in the PCA (Fig. 6) shows that (1) DOM in the mainstem is enriched in the aliphatic fraction compared to its tributaries and (2) the distribution of tributaries for a given Strahler order is strongly heterogeneous. This highlights the combined effects of landscape morphology and water chemistry that can influence the downstream transformation of DOM independently of the size of the streams/rivers. Thus, land cover – here mostly forest and savannah – has a strong influence on the composition of DOM released in aquatic ecosystems (Mann et al., 2014; Lambert et al., 2015), and DOM photodegradation is likely more pronounced in catchments with large open areas as suggested by the lower %C3 in savannah-dominated catchments compared to forest-dominated catchments (Supplementary Fig. 6). Also, a strong connectivity with terrestrial

546 sources can maintain a greater aromatic character to DOM independently of the size of
547 the rivers. This typically refers to the well-known role of wetland areas in delivering large
548 quantities of aromatic DOM in inland waters (Battin et al., 1998; Hanley et al., 2013;
549 Lambert et al., 2016) and thus obscuring variations in DOM occurring upstream. A multi-
550 year monitoring illustrates for example that DOM in the Oubangui River at Bangui (i.e.
551 upstream the Cuvette Centrale, Fig. 1) experiences significant changes in composition
552 between rising waters (June, DOM has few aromatic structures) and high waters
553 (December, DOM is highly aromatic; Bouillon et al., 2014) while our data report highly
554 aromatic DOM during both periods as the river becomes enriched in organic material from
555 the flooded forest (Laraque et al., 2009). Finally, the positive correlations between %C2
556 and pH and between %C6 and pH (Fig. 8) advocate for a limited degree of bacterial
557 degradation of DOM in very acidic environments as previously suggested by Borges et al.
558 (2015a) based on the CO_2 and DOC relationship in the Congo Basin. Such streams and
559 rivers typically correspond to the DOM-rich so-called “black-waters” originating from the
560 Cuvette Centrale, with pH between 3.6 and 5.9 and average 4.4 (Supplementary Fig. 7).
561 **4.3. The chemostat hypothesis and the pulse-shunt concept.** The chemostat
562 hypothesis suggests a decrease in DOC concentrations and a convergence in DOM
563 composition towards lower aromaticity with increasing stream order due to the increasing
564 influence of in-stream processes that overwhelm terrestrial inputs from headwater
565 catchments (Creed et al., 2015). The shift from a predominantly terrestrial influence to
566 biogeochemical processing – assessed by the variation of $SUVA_{254}$ as a function of stream
567 order – has been estimated to occur in third- or fourth-order streams in river networks
568 across the United States (Creed et al., 2015). A net decrease in $SUVA_{254}$ associated with
569 a decrease with DOC concentrations was only found to occur from six to eight order

570 streams in our study (Fig. 9), reflecting the influence of the Cuvette Centrale (i.e. strong
571 connectivity with the flooded dense forest, acidic waters) on the DOM biogeochemistry in
572 the Congo Basin. Although the seasonal variations of water level are modest in the Congo
573 and that the Cuvette Centrale does not flush as floodplain lakes in the Amazon (e.g.
574 Moreira-Turcq et al., 2003), the flooded forest is drained by several large rivers (Ruki,
575 Sangha) that bring large amounts of water and DOM to the mainstem (The Ruki is the
576 second tributary after the Kasai). This falls in line with the "flood pulse concept" of Junk et
577 al. (1989) that highlights the critical importance of the river-floodplain connectivity in
578 lowland tropical rivers (Battin, 1998; Zurbrügg et al., 2013; Lambert et al., 2016), while the
579 chemostat hypothesis builds on the river continuum concept (Vannote et al. 1980) that is
580 typically applicable to rivers at temperate latitudes and devoid of large wetlands. Patterns
581 of other data acquired during the same cruises such as CO_2 and CH_4 also showed the
582 influence of inputs of these quantities from the Cuvette Centrale (Borges et al. 2015a).
583 Also, an increase in DOM content and aromaticity was found to occur in nine order
584 streams, reflecting the fact that DOM-rich waters from the Cuvette Centrale can travel
585 along the ridge of the Congo River without completely mixing with the central water
586 masses of the mainstem (Supplementary Figure 5).

587 Our study also supports the "pulse-shunt" conceptual model that states that the
588 removal of terrestrial DOM in fluvial networks is a function of the hydrological regime of
589 the basin (Raymond et al., 2016). It should be noted that the seasonal variation in water
590 discharge is relatively low in the Congo Basin compared to other large rivers, yet
591 apparently sufficient to significantly impact the degree of DOM photodegradation between
592 FW and HW. The switch between active and passive pipes is likely to be more pronounced
593 in large drainage basins in northern and southern Hemispheres with more contrasting

hydrological regimes, as recently shown in the adjacent Zambezi Basin (Lambert et al., 2016). Our results also suggest that the photodegradation pathway is more sensitive to changes in WRT compared to the biological pathway, but this hypothesis needs to be verified in other environments and by additional incubation experiments.

Data availability

The digital elevation model HydroSHEDS (Lehner et al., 2008) is available at http://hydrosheds.cr.usgs.gov/index.php. The Global Lakes and Wetlands database (Lehner and Döll, 2004) is available at http://www.worldwildlife.org/pages/global-lakes-and-wetlands-database. The Global Land Cover 2009 database is available at http://landcover.usgs.gov/landcoverdata.php.

Acknowledgements

This work was funded by the Fonds National de la Recherche Scientifique (FNRS, TransCongo, 14711103; FluoDOM J.0009.15), the European Research Council (ERC-StG 240002 AFRIVAL), the Belgian Federal Science Policy (BELSPO, COBAFISH, SD/AR/05A), the Research Foundation Flanders (FWO-Vlaanderen), the Research Council of the KU Leuven, and the Fonds Léopold III pour l'Exploration et la Conservation de la Nature. The freshwater discharge data of the Congo at Kinshasa were kindly provided by the Régie des Voies Fluviales (RVF, DRC). We are grateful for help in sampling from T Mambo Baba (Université de Kisangani, DRC), for analytical support from S Petrovic (University of Liège), B Leporcq (University of Namur), and Z Kelemen and C Morana (KU Leuven). We thank two anonymous reviewers for constructive comments on

617 the previous version of the manuscript. TL and AVB are a postdoctoral researcher and
618 senior research associate, respectively, at the FNRS.

619

620 **Author Contributions**

621 A.V.B., F.D., S.B. designed the study; A.V.B., and F.D. collected the field data; S.B. and
622 T.L. performed sample analysis; T.L. carried out the geographical system information
623 (GIS) analysis and performed the PARAFAC model with help of P.M.; T.L. analyzed the
624 data and drafted the manuscript that was revised and approved by all co-authors.

625 **References**

626 Baines, S. B. and Pace, M. L.: The production of dissolved organic matter by
627 phytoplankton and its importance to bacteria: patterns across marine and freshwater
628 systems, Limnol. Oceanogr., 36, 1078–1090, 1991.

629 Bano, N., Moran, M. A., and Hodson, R. E.: Photochemical formation of labile organic
630 matter from two components of dissolved organic carbon in a freshwater wetland,
631 Aquat. Microb. Ecol., 16, 95–102, 1998.

632 Battin, T. J., Kaplan, L. A., Findlay, S., Hopkinson, C. S., Marti, E., Packman, A. I.,
633 Newbold, J. D., and Sabater, F.: Biophys- ical controls on organic carbon fluxes in
634 fluvial networks, Nat. Geosci., 1, 95–100, 2008.

635 Battin, T. J.: Dissolved organic matter and its optical properties in a blackwater tributary
636 of the upper Oricono river, Venezuela, Org. Geochem., 28, 561-569,1998.

637 Berggren, M., Lapierre, J.-F., and del Giorgio, P. A.: Magni- tude and regulation of
638 bacterioplankton respiratory quotient across freshwater environmental gradients,
639 ISME J., 6, 984–993, doi:10.1038/ismej.2011.157, 2012.

640 Bertilsson, S. and Jones, J. B.: Supply of dissolved organic matter to aquatic ecosystems:
641 autochthonous sources, in: Aquatic ecosystems: interactivity of dissolved organic
642 matter, Findlay, S., & Sinsabaugh, R. L. (Eds.), Academic Press, 3 – 24, 2003.
643 Besemer, K., Luef, B., Preiner, S., Eichberger, B., Agis, M., and Peduzzi, P.: Sources and
644 composition of organic matter for bacterial growth in a large European river
645 floodplain system (Danube, Austria), Org. Geochem., 40, 321–331, 2009.
646 Bontemps, S., Defourney, P., Van Bogaert, E., and Arino, O.: GLOBCOVER2009
647 Products Description and Validation Report. (ESA and UCLouvain) (available online
648 at http://ionia1.esrin.esa.int/docs/GLOBCOVER2009_Validation_Report_2.2.pdf),
649 2010 (Accessed: 15 September 2015).
650 Borcard, D., Gillet, F., and Legendre, P.: Numerical ecology with R, Springer New York,
651 New York, 306 pp., doi.org/10.1007/978-1-4419-7976-6, 2011.
652 Borges, A. V., Darchambeau, F., Teodoru, C. R., Marwick, T. R., Tamooh, F., Geeraert,
653 N., Omengo, F. O., Guerin, F., Lambert, T., Morana, C., Okuku, E., and Bouillon, S.:
654 Globally significant greenhouse-gas emissions from African inland waters, Nature
655 Geosci., 8, 637-642, doi:10.1038/ngeo2486, 2015a.
656 Borges, A. V., Abril, G., Darchambeau, F., Teodoru, C. R., Deborde, J., Vidal, L. O.,
657 Lambert, T., and Bouillon, S.: Divergent biophysical controls of aquatic CO_2 and CH_4
658 in the World's two largest rivers; Sci. Rep., 5, 15614, doi: 10.1038/srep15614, 2015b.
659 Bouillon, S., Yambélé, A., Gillikin, D. P., Teodoru, C. R., Darchambeau, F., Lambert, T.,
660 and Borges, A. V.: Contrasting biogeochemical characteristics of the Oubangui River
661 and tributaries (Congo River basin), Sci. Rep., 4, 1–10, doi:10.1038/srep05402,
662 2014.

663 Bouillon, S., Yambélé, A., Spencer, R. G. M., Gillikin, D. P., Hernes, P. J., Six, J., Merckx,
664 R., and Borges, A.V.: Organic matter sources, fluxes and greenhouse gas exchange
665 in the Oubangui River (Congo River basin), Biogeosciences, 9, 2045–2062,
666 doi:10.5194/bg-9-2045-2012, 2012.
667 Bricquet, J. P. : Les écoulements du Congo à Brazzaville et la spatialisation des apports,
668 in Grands Bassins Fluviaux Péri-atlantiques, edited by J. C. Olivry and J. Boulègue,
669 pp. 27–38, Inst. Fr. de Rech. Sci.pour le Dev. en Coop. (ORSTOM), Paris, 1995.
670 Bwangoy, J.-R. B., Hansen, M. C., Roy, D. P., De Grandi, G. and Justice, C. O.: Wetland
671 mapping in the Congo Basin using optical and radar remotely sensed data and
672 derived topographical indices, Remote Sens. Environ., 114, 73–86, 2010.
673 Cawley, K. M., Wolski, P., Mladenov, N., and Jaffé, R.: Dissolved organic matter
674 biogeochemistry along a transect of the Okavango delta, Bostwana, Wetlands, 32,
675 475–486, doi: 10.1007/s13157-012-0281-0, 2012.
676 Coble, P. G., Lead, J., Baker, A., Reynolds, D. M., and Spencer, R. G. M.: Aquatic Organic
677 Matter Fluorescence, NY: Cambridge University Press, New York, 375 pp., 2014.
678 Cole, J. J., Prairie, Y. T., Caraco, N. F., McDowell, W. H., Tranvik, L. J., Striegl, R. G.,
679 Duarte, C. M., Kortelainen, P., Downing, J. A., Middelburg, J. J., and Melack, J.:
680 Plumbing the global carbon cycle: integrating inland waters into the terrestrial carbon
681 budget, Ecosystems, 10, 171–184, 2007.
682 Cory, R. M., Harrold, K. H., Neilson, B. T., and King, G. W.: Controls on dissolved organic
683 matter (DOM) degradation in a headwater stream: the influence of photochemical
684 and hydrological conditions in determining light-limitation or substrate-limitation of
685 photo-degradation, Biogeosciences, 12, 6669-6685, doi:10.5194/bg-12-6669-2015,
686 2015.

687 Cory, R. M., McKnight, D. M., Chin, Y. P., Miller, P., and Jaros, C. L.: Chemical
688 characteristics of fulvic acids from Arctic surface waters: Microbial contributions and
689 photochemical transformations, J. Geophys. Res.-Biogeosci., 112, G04S51,
690 doi:10.1029/2006JG000343, 2007.
691 Cory, R. M., Ward, C. P., Crump, B. C., and Kling, G. W.: Sunlight controls water column
692 processing of carbon in arctic freshwaters, Science, 345, 925–928,
693 doi:10.1126/science.1253119, 2014.
694 Coynel, A., Seyler, P., Etcheber, H., Meybeck, M., and Orange, D.: Spatial and seasonal
695 dynamics of total suspended sediment and organic carbon species in the Congo
696 River, Global Biogeochem. Cy., 19, GB4019, doi:10.1029/2004GB002335, 2005.
697 Creed, I. F., McKnight, D., Pellerin, B. A., Green, M. B., Bergamaschi, B. A., Aiken, G. R.,
698 Burns, D. A., Findlay, S. E. G., Shanley, J. B., Striegl, R. G., Aulenbach, B. T., Clow,
699 D. W., Laudon, H., McGlynn, B. L., McGuire, K. J., Smith, T. A., and Stackpoole, S.
700 M.: The river as a chemostat: fresh perspectives on dissolved organic matter flowing
701 down the river continuum, Can. J. Fish. Aquat. Sci., 72, 1272–1285,
702 dx.doi.org/10.1139/cjfas-2014-0400, 2015.
703 Descy, J.P., Darchambeau, F., Lambert, T., Stoyneva, M.P., Bouillon, S., and Borges,
704 A.V.: Phytoplankton dynamics in the Congo River, in press.
705 Fasching, C., Behounek, B., Singer, G. A., and Battin, T. J.: Microbial degradation of
706 terrigenous dissolved organic matter and potential consequences for carbon cycling
707 in brown-water streams, Scientific reports, 4, doi:10.1038/srep04981, 2014.
708 Fellman, J. B., Hood, E., and Spencer, R. G. M.: Fluorescence spectroscopy opens new
709 windows into dissolved organic matter dynamics in freshwater ecosystems: A
710 review, Limnol. Oceanogr., 55, 2452–2462, doi:10.4319/lo.2010.55.6.2452, 2010.

711 Guillemette, F. and del Giorgio, P. A.: Simultaneous consumption and production of
712 fluorescent dissolved organic matter by lake bacterioplankton, Environ. Microbiol.,
713 14, 1432–1443.
714 Hanley, K., Wollheim, W. M., Salisbury, J., Huntington, T., and Aiken, G.: Controls on
715 dissolved organic carbon quantity and chemical character in temperate rivers of
716 North America, Global Biogeochem. Cy., 27, 492–504, doi:10.1002/gbc.20044,
717 2013.
718 Helms, J. R., Stubbins, A., Ritchie, J. D., Minor, E. C., Kieber, D. J., and Mopper, K.:
719 Absorption spectral slopes and slope ratios as indicators of molecular weight,
720 source, and photobleaching of chromophoric dissolved organic matter, Limnol.
721 Oceanogr., 53, 955–969, 2008.
722 Ishii, S. K. L. and Boyer, T. H.: Behavior of reoccurring parafac components in fluorescent
723 dissolved organic matter in natural and engineered systems: A critical review,
724 Environ. Sci. Tech- nol. 46, 2006–2017, doi:10.1021/es2043504, 2012.
725 Jaffé, R., McKnight, D., Maie, N., Cory, R., McDowell, W. H., and Campbell, J. L.: Spatial
726 and temporal variations in DOM composition in ecosystems: The importance of long-
727 term monitoring of optical properties, J. Geophys. Res.-Biogeo., 113, G04032,
728 doi:10.1029/2008jg000683, 2008.
729 Junk, W., Bayley, P. B., and Sparks, R. E.: The flood pulse concept in river-floodplain
730 systems, Can. Spec. Publ. Fish. Aquat. Sci., 106, 110–127, 1989.
731 Kellerman, A. M., Kothawala, D. N., Dittmar, T., and Tranvik, L. J.: Persistence of
732 dissolved organic matter in lakes related to its molecular characteristics, Nat.
733 Geosci., 8, 454–457, doi: 10.1038/ngeo2440, 2015.

Kothawala, D. N., Stedmon, C. A., Müller, R. A., Weyhenmeyer, G. A., Köhler, S. J., and Tranvik, L. J.: Controls of dissolved organic matter quality: Evidence from a large-scale boreal lake survey, Glob. Change Biol., 20, 1101–1114, doi:10.1111/gcb.12488, 2014.

Lambert, T., Pierson-Wickmann, A.-C., Gruau, G., Thibault, J. N., and Jaffrezic, A.: Carbon isotopes as tracers of dissolved organic carbon sources and water pathways in headwater catchments, J. Hydrol., 402, 228–238, doi:10.1016/j.jhydrol.2011.03.014, 2011.

Lambert, T., Darchambeau, F., Bouillon, S., Alhou, B., Mbega, J- D, Teodoru, C. R., Nyoni, F. C., Massicotte, P., and A V Borges, A. V.: Landscape control on the spatial and temporal variability of chromophoric dissolved organic matter and dissolved organic carbon in large African rivers, Ecosystems, 18, 1224–1239, doi:10.1007/s10021-015-9894-5, 2015.

Lambert, T., Teodoru, C. R., Nyoni, F., Bouillon, S., Darchambeau, F., Massicotte, P., and Borges, A. V.: Along-stream transport and transformation of dissolved organic matter in a large tropical river, Biogeosciences, 13, 1–15, doi:10.5194/bg-13-1-2016, 2016.

Lapierre, J. F. and del Giorgio, P.A.: Partial coupling and differential regulation of biologically and photochemically labile dissolved organic carbon across boreal aquatic networks, Biogeosciences, 11, 5969–5985, doi:10.5194/bg-11-5969-2014, 2014.

Laraque, A., Bricquet, J. P., Pandi, A., and Olivry, J. C.: A review of material transport by the Congo River and its tributaries, Hydrol. Process., 23, 3216–3224, 2009.

Leenheer, J. and Croué, J.: Characterizing aquatic dissolved organic matter, Environ. Sci. Technol., 37, 18 – 26, 2003.

758 Lehner, B. and Döll, P.: Development and validation of a global database of lakes,
759 reservoirs and wetlands, J. Hydrol., 296, 1–22, doi:10.1016/j.jhydrol.2004.03.028,
760 2004.
761 Lehner, B., Verdin, K., and Jarvis, A.: New global hydrography derived from space borne
762 elevation data, Eos, 89, 93–94, 2008.
763 Mann, P.J., Spencer, R. G. M., Dinga, B. J., Poulsen, J.R., Hernes, P.J., Fiske, G., Salter,
764 M. E., Wang, Z. A., Hoering, K.A., Six, J., and Holmes, R. M.: The biogeochemistry
765 of carbon across a gradient of streams and rivers within the Congo Basin. J.
766 Geophys. Res.-Biogeo., 119, 687–702, 2014.
767 Marín-Spiotta, E., Gruley, K. E., Crawford, J., Atkinson, E. E., Miesel, J. R., Greene, S.,
768 Cardona-Correa, C., and Spencer, R. G. M.: Paradigm shifts in soil organic matter
769 research affect interpretations of aquatic carbon cycling: transcending disciplinary
770 and ecosystem boundaries, Biogeochemistry, 117, 279-297, doi: 10.1007/s10533-
771 013-9949-7, 2014.
772 Massicotte, P. and Frenette, J.-J.: Spatial connectivity in a large river system: resolving
773 the sources and fate of dissolved organic matter, Ecol. Appl., 21, 2600–2617, 2011.
774 McKnight, D. M., Boyer, E. W., Westerhoff, P. K., Doran, P. T., Kulbe, T., and Andersen,
775 D. T.: Spectrofluorometric characterization of dissolved organic matter for indication
776 of precursor organic material and aromaticity, Limnol. Oceanogr., 46, 38–48, 2001.
777 Meybeck, M.: Riverine transport of atmospheric carbon: source, global typology and
778 budget. Water, Air, and Soil Pollution, 70, 443–463, 1993.
779 Morana, C., Sarmento, H., Descy, J.-P., Gasol, J.M., Borges, A. V., Bouillon, S., and
780 Darchambeau, F.: Production of dissolved organic matter by phytoplankton and its

781 uptake by heterotrophic prokaryotes in large tropical lakes, Limnol. Oceanogr., 59,
782 1364 – 1375, 2014.
783 Moreira-Turcq, P., Seyler, P., Guyot, J. L., and Etcheber, H.: Exportation of organic carbon
784 from the Amazon River and its main tributaries, Hydrol. Process., 17, 1329–1344,
785 2003.
786 Murphy, K. R., Stedmon, C. A., Graeber, D. and Bro, R.: Fluorescence spectroscopy and
787 multi-way techniques. PARAFAC. Anal. Methods 5, 6557–6566, 2013.
788 Neff, J. C., Finlay, J. C., Zimov, S. A., Davydov, S. P., Car- rasco, J. J., Schuur, E. A. G.,
789 and Davydova, A. I.: Seasonal changes in the age and structure of dissolved organic
790 carbon in Siberian rivers and streams, Geophys. Res. Lett., 33, L23401,
791 doi:10.1029/2006GL028222, 2006.
792 Ohno, T.: Fluorescence inner-filtering correction for determining the humification index of
793 dissolved organic matter, Environ. Sci. Technol., 36, 742–746,
794 doi:10.1021/Es0155276, 2002.
795 Osburn, C.L., Retamal, L., and Vincent, W.F.: Photoreactivity of chromophoric dissolved
796 organic matter transported by the Mackenzie River to the Beaufort Sea. Mar. Chem.
797 115, 10–20, doi: 10.1016/j.marchem.2009.05.003, 2009.
798 Poole, G. C.: Stream hydrogeomorphology as a physical science basis for advances in
799 stream ecology, J. N. Am. Benthol. Soc., 29, 12–25, 2010.
800 Raymond, P. A., Saiers, J. E., and Sobczak W. V.: Hydrological and biogeochemical
801 controls on watershed dissolved organic matter transport: pulse-shunt concept,
802 Ecology, 97, 5–16, doi.org/10.1890/14-1684.1, 2016.
803 Remington, S., Krusche, A., and Richey, J.: Effects of DOM photochemistry on bacterial
804 metabolism and CO_2 evasion during falling water in a humic and a whitewater river

805 in the Brazilian Amazon, Biogeochemistry, 105, 185–200, doi: 10.1007/s10533-010-
806 9565-8, 2011.
807 Richardson, D. C., Newbold, J. D., Aufdenkampe, A. K., Taylor, P. G., and Kaplan, L. A.:
808 Measuring heterotrophic respiration rates of suspended particulate organic carbon
809 from stream ecosystems, Limnol. Oceanogr.-Meth., 11, 247–261, 2013.
810 Runge, J.: The Congo River, Central Africa in Large Rivers: Geomorpholgy and
811 Management, Ed. Gupta, A., John Wiley & Sons, Ltd, 293–309, 2008.
812 Sanderman, J., Lohse, K. A., Baldock, J. A., and Amundson, R.: Linking soils and streams:
813 sources and chemistry of dissolved organic matter in a small coastal
814 watershed,Water Resour. Res., 45, W03418, doi:10.129/2008WR006977, 2009.
815 Spencer, R. G. M., Stubbins, A., Hernes, P. J., Baker, A., Mopper, K., Aufdenkampe, A.
816 K., Dyda, R. Y., Mwamba, V. L., Mangangu, A. M., Wabakanghanzi, J. N., and Six,
817 J.: Photochemical degradation of dissolved organic matter and dissolved lignin
818 phenols from the Congo River, J. Geophys. Res.-Biogeo., 114,
819 doi:10.1029/2009jg000968, 2009.
820 Spencer, R. G. M., Hernes, P. J., Ruf, R., Baker, A., Dyda, R. Y., Stubbins, A., and Six,
821 J.: Temporal controls on dissolved organic matter and lignin biogeochemistry in a
822 pristine tropical river, Democratic Republic of Congo, J. Geophys. Res., 115,
823 G03013, doi:10.1029/2009JG001180, 2010.
824 Spencer, R. G. M., Hernes, P. J., Aufdenkampe, A. K., Baker, A., Gulliver, P., Stubbins,
825 A., Aiken, G. R., Dyda, R. Y., Butler, K. D., Mwamba, V. L., Mangangu, A. M.,
826 Wabakanghanzi, J. N., and Six, J.: An initial investigation into the organic matter bio-
827 geochemistry of the Congo River, Geochim. Cosmochim. Acta, 84, 614–627, 2012.

828 Stedmon, C. A. and Markager, S.: Resolving the variability in DOM fluorescence in a
829 temperate estuary and its catchment unsing PARAFAC, Limnol.Oceanogr, 50, 686–
830 697, 2005.
831 Stedmon, C. A., Markager, S., and Bro, R.: Tracing dissolved organic matter in aquatic
832 environments using a new approach to fluorescence spectroscopy, Mar. Chem., 82,
833 239–254, doi:10.1016/s0304-4203(03)00072-0, 2003.
834 Strahler, A.N.: Quantitative analysis of watershed geomorphology, T. Am. Geophys.
835 Union, 38, 913–920, 1957.
836 Stubbins, A., Lapierre, J.F., Berggren, M., Prairie, Y.T., Dittmar, T., and del Giorgio, P.A.:
837 What's in an EEM? Molecular signatures associated with dissolved organic
838 fluorescence in boreal Canada, Environ Sci. Technol., 48, 10598–10606, 2014.
839 Tranvik, L. J. and Bertilsson, S.: Contrasting effects of solar UV radiation on dissolved
840 organic sources for bacterial growth, Ecol. Lett., 4, 458–463, 2001.
841 Vannote, R. L., Minshall, G. W., Cummins, K. W., Sedell, J. R., and Cushing, C. E.: The
842 river continuum concept, Can. J. Fish. Aquat. Sci., 37, 130–137, 1980.
843 Wagner, S., Jaffé , R., Cawley, K., Dittmar, T., and Stubbins, A.: Associations Between
844 the Molecular and Optical Properties of Dissolved Organic Matter in the Florida
845 Everglades, a Model Coastal Wetland System. Front. Chem. 3:66. doi:
846 10.3389/fchem.2015.00066, 2015.
847 Walker, S. A., Amon, R. M., and Stedmon, C. A.: Variations in high-latitude riverine
848 fluorescent dissolved organic matter: A comparison of large Arctic rivers, J.
849 Geosphys. Res-Biogeo., 118, 1689–1702, doi:10.1002/2013JG002320, 2013.
850 Ward, N. D., Keil, R. G., Medeiros, P. M., Brito, D. C., Cunha, A. C., Dittmar, T., Yager, P.
851 L., Krusche, A. V., and Richey, J. E.: Degradation of terrestrially derived

852 macromolecules in the Amazon River, Nat. Geosci., 6, 530–533,
853 doi:10.1038/ngeo1817, 2013.
854 Weishaar, J. L., Aiken, G. R., Bergamaschi, B. A., Fram, M. S., Fujii, R., and Mopper, K.:
855 Evaluation of specific ultraviolet absorbance as an indicator of the chemical
856 composition and reactivity of dissolved organic carbon, Environ. Sci. Technol., 37,
857 4702–4708, doi: 10.1021/es030360x, 2003.
858 Weyhenmeyer, G. A., Fröberg, M., Karltun, E., Khalili, M., Kothawala, D., Temnerud, J.,
859 and Tranvik, L. J.: Selective decay of terrestrial organic carbon during transport from
860 land to sea, Glob. Change Biol., 18, 349–355, doi:10.1111/j.1365-
861 2486.2011.02544.x, 2012.
862 Yamashita, Y., Scinto, L. J., Maie, N., and Jaffé, R.: Dissolved organic matter
863 characteristics across a subtropical wetland's landscape: application of optical
864 properties in the assessment of environmental dynamics, Ecosystems, 13, 1006–
865 1019, doi:10.1007/s10021-010-9370-1, 2010.
866 Zepp, R. G., Sheldon, W. M., and Moran, M. A.: Dissolved organic fluorophores in
867 southeastern US coastal waters: correction method for eliminating Rayleigh and
868 Raman scattering peaks in excitation–emission matrices, Mar. Chem., 89, 15–36,
869 doi:10.1016/j.marchem.2004.02.006, 2004.
870 Zurbrügg, R., Suter, S., Lehmann, M. F., Wehrli, B., and Senn, D. B.: Organic carbon and
871 nitrogen export from a tropical dam-impacted floodplain system, Biogeosciences, 10,
872 23–38,doi:10.5194/bg-10-23-2013, 2013.

Figures captions

Figure 1 – Maps of the Congo Basin showing (a) the elevation (Lehner et al., 2008), the main hydrological network, the extent of the Cuvette Centrale (Lehner and Döll, 2004), the distribution of sampling sites along the Kisangani – Kinshasa transect and (b) the dominant land cover (Bontemps et al., 2011). The red line "A" indicates the entrance of the Congo River within the core of the Cuvette Centrale (see text for details and supplementary figure 1).

Figure 2 – Average freshwater discharge of the Congo River, and corresponding water height at the gauging station at (a) Kisangani for the period 2013-2016, and (b) Kinshasa for the period 2003-2013. Timing of the two cruises is indicated by thicker lines.

Figure 3 – Longitudinal evolution of DOM properties in the mainstem, large and small tributaries along the Kisangani-Kinshasa transect during HW (left panels) and FW (right panels). From top to bottom the panels represent: DOC, $\delta^{13}C_{DOC}$, $SUVA_{254}$, S_R and FI. Numbers refer to large tributaries: (1) the Kwa/Kasai, (2) the Lefini, (3) the Sangha, (4) the Oubangui, (5) the Ruki, (6) the Ikelemba, (7) the Lulonga, (8) the Mongala, (9) the Itimbiri, (10) the Aruwini, (11) the Lomami, (12) the Lindi and (13) the Tshopo River.

Figure 4 – Relationships between DOC concentrations in tributaries and the extent of flooded dense forest.

Figure 5 – Longitudinal evolution of the relative contribution of PARAFAC component in the mainstem, large and small tributaries along the Kisangani-Kinshasa transect during HW (left panels) and FW (right panels).

Figure 6 – Graphical representation of PCA results, including loadings plot for the input variables and scores plot for stations based on (a) their Strahler stream order or (b) sampling location. PCA results based on the hydrological period is included in each plot.

Figure 7 – (a) Relationship between %C5 and %C3 and (b) relationships between %C5 and pelagic community respiration (R) in the Congo Basin.

Figure 8 – Relationship between the relative contribution of aliphatic components (C2 and C6) and pH of stream waters in the Congo Basin.

Figure 9 – DOC concentrations and DOM aromaticity ($SUVA_{254}$) across a gradient of streams and rivers in the Congo Basin as a function of stream order. The box spans the interquartile range (25–75 percentiles), whiskers correspond to min-max values, horizontal bar to median, cross to average.

905

906 **Table 1 –** Selected attributes (mean±standard deviation, min-max) of sampling sites
907 during the field campaigns: oxygen saturation level (%O_2), pH, Secchi depth, vertical light
908 attenuation coefficient (K_d), total suspended matter (TSM) and Chlorophyll-a (Chla)
909 concentrations (data from Descy et al. 2016).

Period	n	%O_2 (%)	pH	Secchi (cm)	K_d (m^{-1})	TSM (mg L^{-1})	Chla (µg L^{-1})
Maximum high waters							
Mainstream	35	60.3±10.6 (48.4-89.2)	6.46±0.22 (6.07-6.92)	54.6±15.6 (25-80)	1.5±0.4 (1.0-2.8)	29.4±21.9 (14.0-99.8)	0.84±0.42 (0.10-1.76)
Major tributaries	13	54.3±33.3 (8.6-111.3)	5.67±1.09 (3.91-6.87)	79.5±60.7 (25-250)	1.5±0.6 (0.4-2.5)	12.5±13.3 (0.74-44.4)	0.54±1.02 (0.01-3.57)
Minor tributaries	26	27.9±30.2 (4.2-99.8)	5.33±0.75 (3.91-6.17)	86.2±29.7 (15-140)	1.5±0.5 (0.9-2.8)	7.7±13.4 (1.7-71.4)	0.35±0.42 (0-1.85)
Falling waters after second peak water discharge							
Mainstream	34	84.8±7.4 (54.2-93.4)	6.82±0.32 (6.08-7.38)	46.8±5.7 (35-62)	3.9±0.6 (1.5-4.6)	31.9±9.1 (4.0-45.4)	3.99±1.54 (1.13-7.68)
Major tributaries	12	62.1±31.2 (0.3-98.2)	5.77±1.22 (3.63-7.05)	66.7±23.4 (35-106)	3.3±0.7 (2.4-5.1)	14.4±12.5 (0.73-43.0)	1.65±2.27 (0.02-6.39)
Minor tributaries	41	37.8±35.6 (0.3-103.0)	4.56±0.77 (3.6-6.1)	80.7±42.2 (38-205)	3.3±0.9 (1.5-5.2)	6.1±6.5 (0.5-34.8)	0.55±0.99 (0.01-5.12)

910

911 **Table 2 –** Spectral properties (excitation and emission maxima (Ex_{max}/Em_{max})) of the six components identified using
912 PARAFAC modelling, correspondence with peak classification, general assignment and comparison with previously
913 identified components in different environments, dominant molecular association and possible source and reactivity.
914 Dominant molecular association is based on FTICR-MS studies. Numbers in brackets refer to the second peak of maximal
915 excitation.

Component	Ex_{max} (nm)	Em_{max} (nm)	Peak(s) name[1]	General assignment[2]	Comparison with others environments							Dominant molecular association[4,6,10]	Potential sources and reactivity*
					Arctic Rivers[3]	St Lawrence River[4]	Boreal streams[5,6]	Boreal lakes[7,8]	Tropical wetland[9,10]	Zambezi basin[11]	Tropical wetland[12]		
C1	<260 (375)	488	A+/C+	Terrestrial humic-like	C3	C3	C2	C3	C5	C2	C2	High aromaticity, high MW	T^{1-12}, $P-^{5}$
C2	305 (<260)	414	M	Microbial humic-like	—	C7	C5	C2	C4	C3	C3	Aliphatic, low MW	$M+^{8-10}$
C3	330 (<260)	444	A_C/C	Terrestrial humic-like	C1	C2	C3	C1	C6	C1	C1	High aromaticity, high MW	T^{1-12}, $P-^{5,9,10}$
C4	<260	444	A_C	Terrestrial humic-like	—	C1	—	C5	C2	C4	—	Aromatic, intermediate MW	T^{9-11}, $P+^{4}$, Pr^{10}
C5	350	424	C	Humic-like	—	—	C4	—	—	—	—	Low aromaticity, low MW	$P+^{5}$
C6	275	350	B/T	Tryptophan-like	C5	C4	C6	C6	C7	C5	C4	Aliphatic, low MW	$Au^{4,9,11}$, $M+^{3,7}$, $M-^{5}$

(1) Coble et al., 2014; (2) Fellman et al., 2010; (3) Walker et al., 2013; (4) Massicotte and Frenette, 2011; (5) Lapierre and del Giorgio, 2014; (6) Stubbins et al., 2014 (FTICR-MS); (7) Kothawala et al., 2014; (8) Kellerman et al., 2015 (FTICR-MS); (9) Yamashita et al., 2010; (10) Cawley et al., 2012; (11) Lambert et al., 2016; (12) Wagner et al., 2015 (FTICR-MS)
*Au: autochtonous production; T: terrestrial inputs; M+: microbial dregradation; M-: biolabile; P+: photoproduct; Pr:photo-resistant; P-: photosensible

916

Figure 1

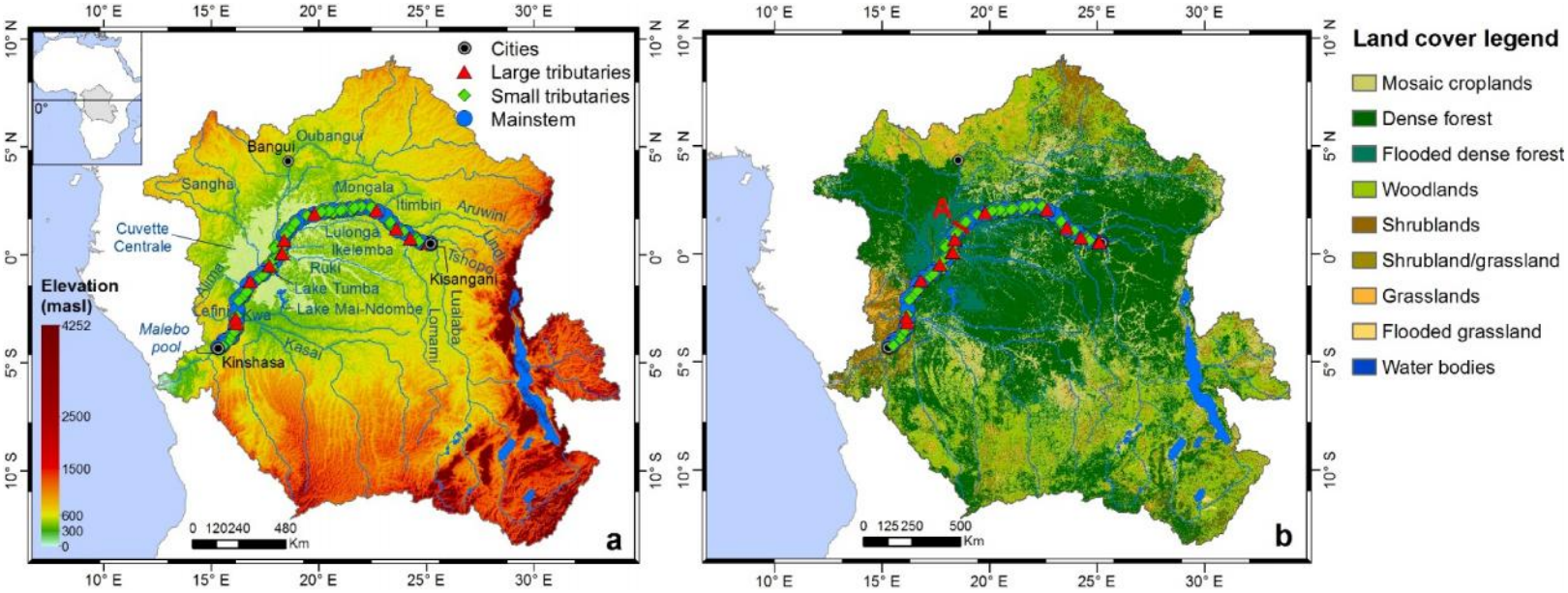
Cities
Large tributaries
Small tributaries
Mainstem
Elevation (masl)
4252
2500
1500
600
300
0
Bangui
Oubangui
Sangha
Mongala
Itimbiri
Aruwimi
Cuvette Centrale
Luonga
Ikelemba
Ruki
Lake Tumba
Lake Mai-Ndombe
Kisangani
Tshopo
Lindi
Lulaba
Lomami
Kasai
Kwa
Kinshasa
Malebo pool
0 120240 480 Km
a
0 125250 500 Km
b
Land cover legend
Mosaic croplands
Dense forest
Flooded dense forest
Woodlands
Shrublands
Shrubland/grassland
Grasslands
Flooded grassland
Water bodies

920 **Figure 2**

921

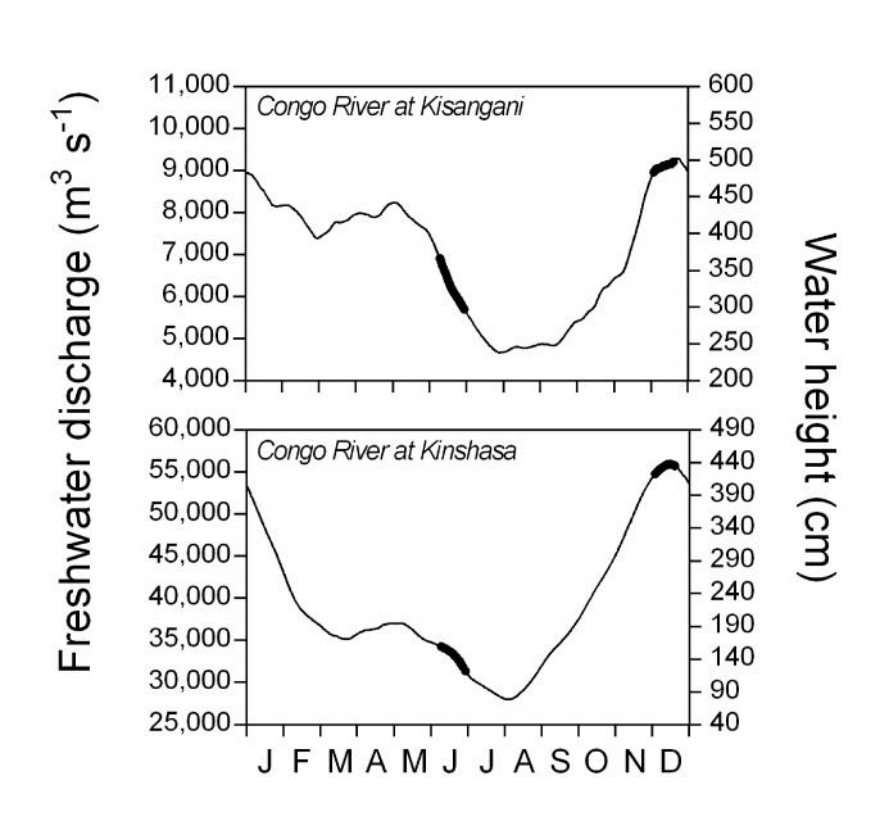

922

923 **Figure 3**

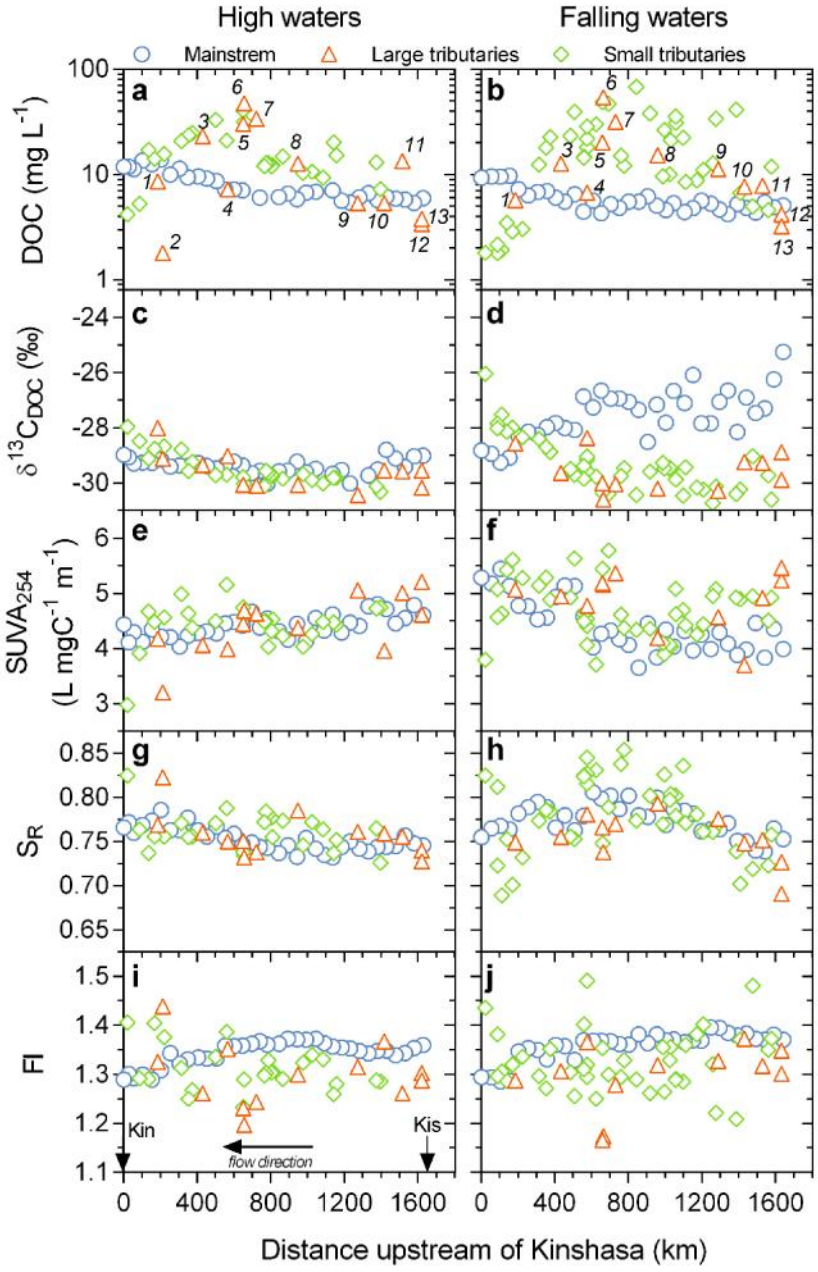

924

925 **Figure 4**

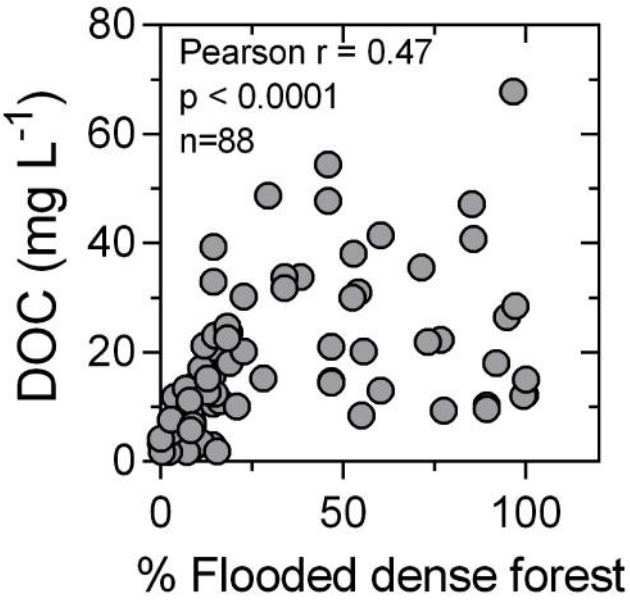

926

927 **Figure 5**

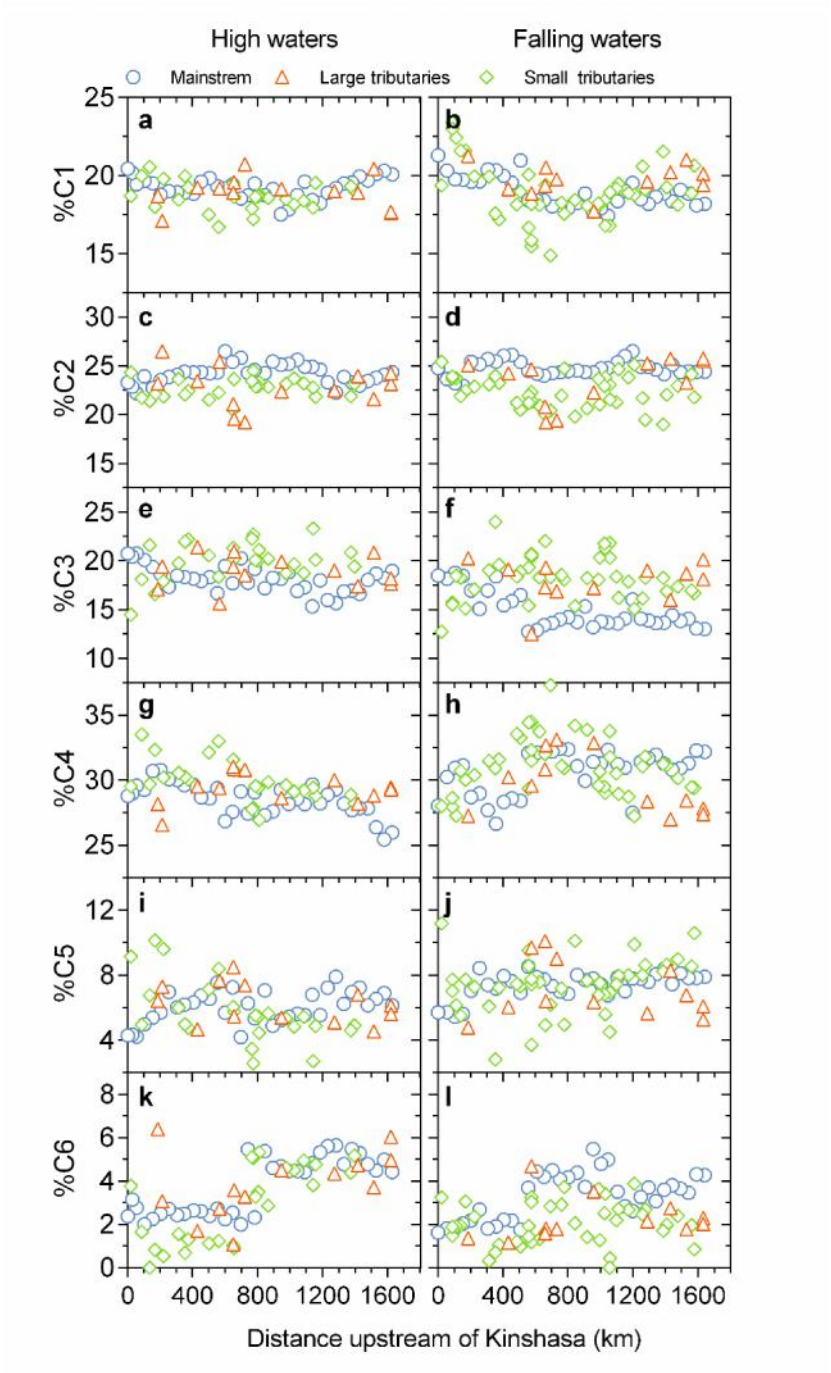

928

929 **Figure 6**

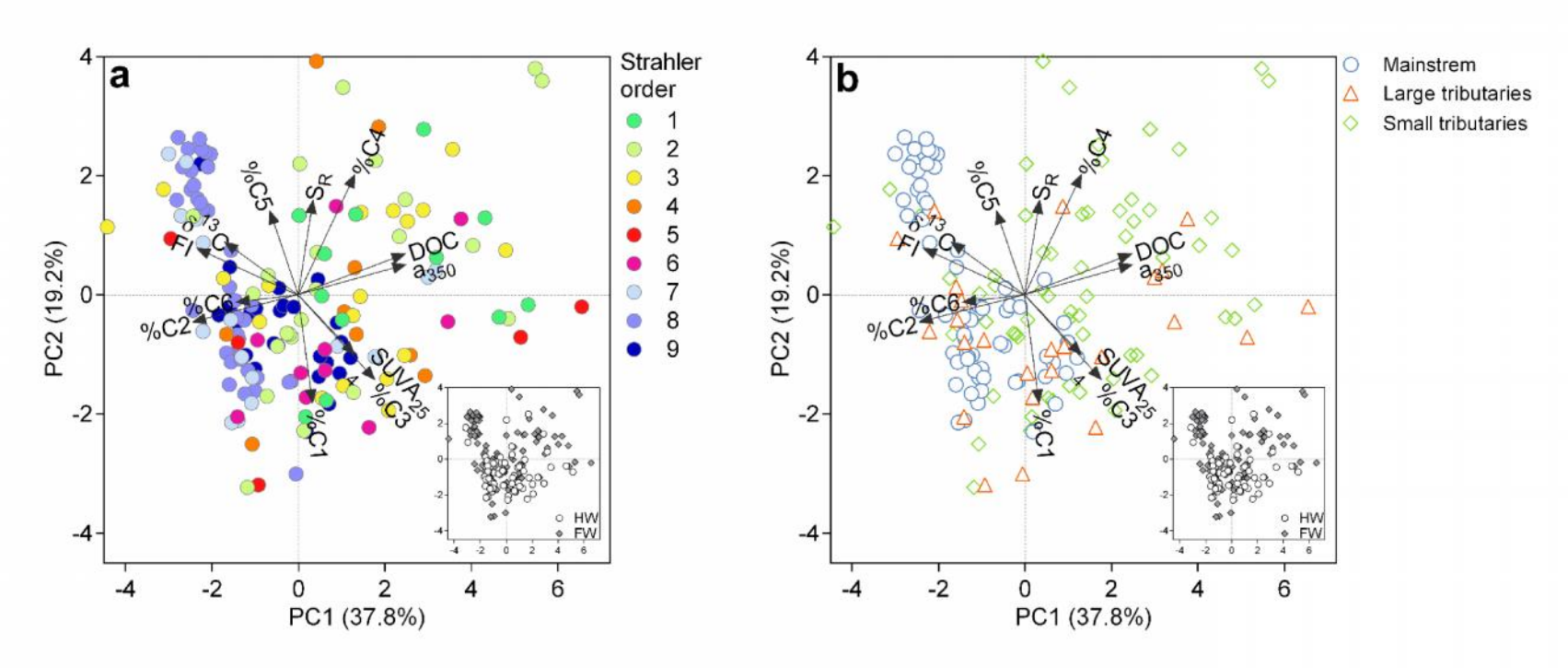

930

931 **Figure 7**

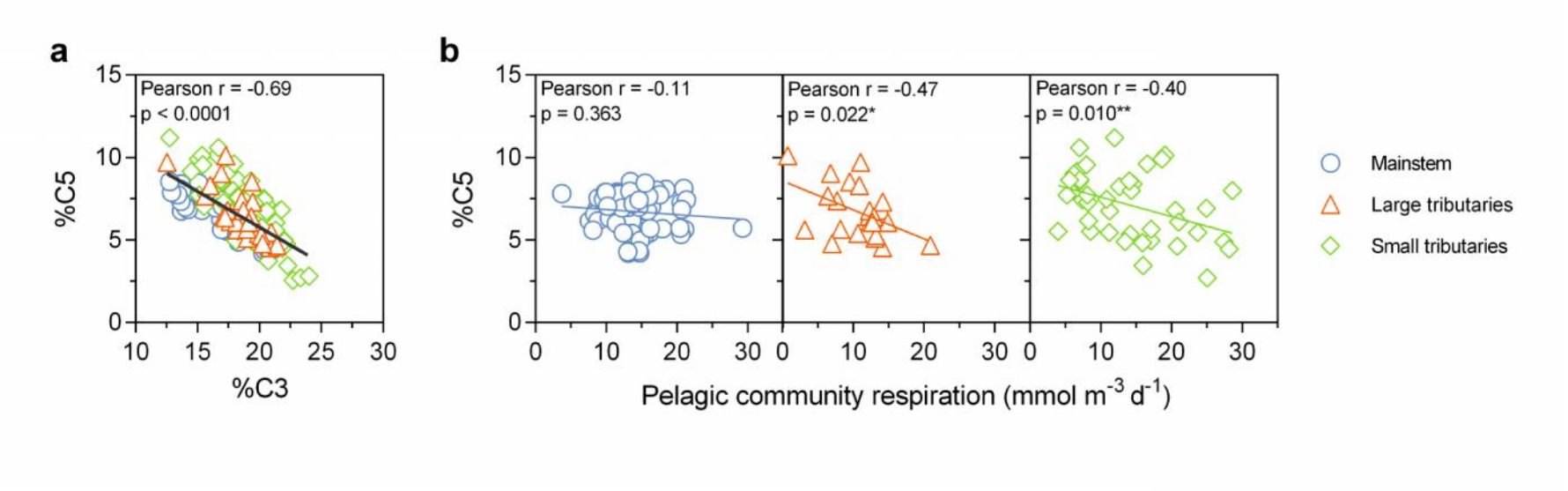

932

933 **Figure 8**

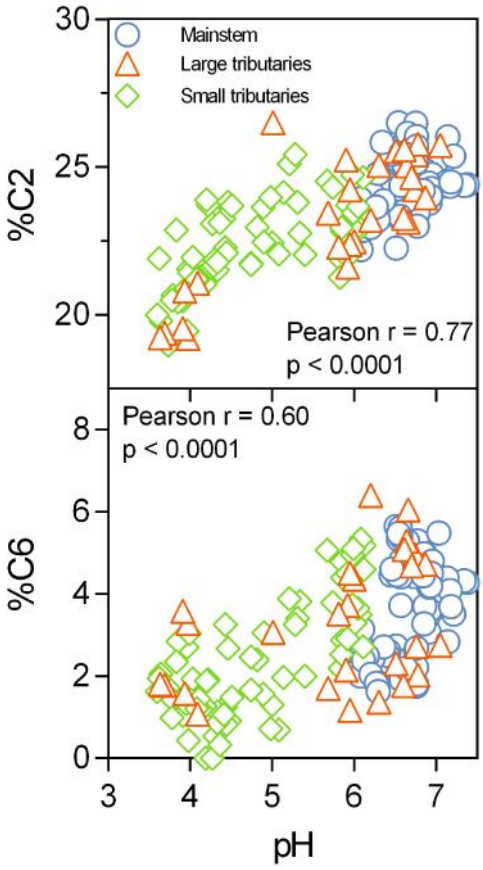

934

935 **Figure 9**

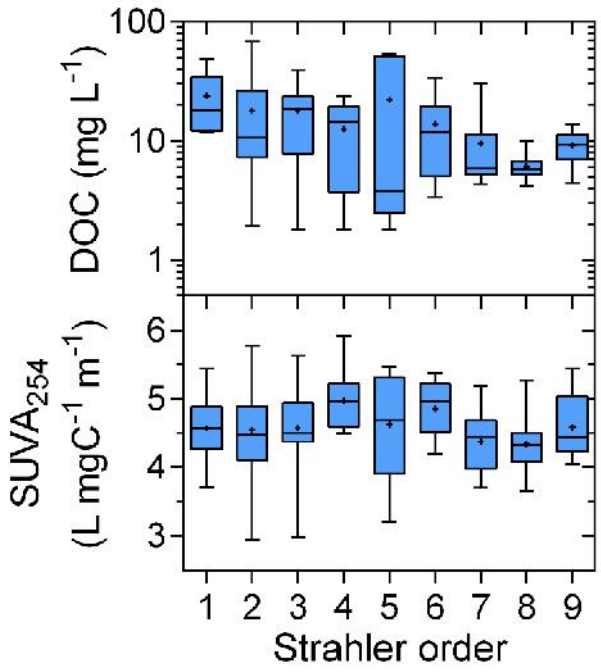

936